



## City Research Online

### City, University of London Institutional Repository

---

**Citation:** Fonseca, J., Reyes-Aldasoro, C. C., O'Sullivan, C. & Coop, M. R. (2015). Experimental investigation into the primary fabric of stress transmitting particles. In: Soga, K., Kumar, K., Biscontin, G. & Kuo, M. (Eds.), *Geomechanics from Micro to Macro*. (pp. 1019-1024). London, UK: CRC Press. ISBN 9781138027077

This is the accepted version of the paper.

This version of the publication may differ from the final published version.

---

**Permanent repository link:** <https://openaccess.city.ac.uk/id/eprint/4138/>

**Link to published version:**

**Copyright:** City Research Online aims to make research outputs of City, University of London available to a wider audience. Copyright and Moral Rights remain with the author(s) and/or copyright holders. URLs from City Research Online may be freely distributed and linked to.

**Reuse:** Copies of full items can be used for personal research or study, educational, or not-for-profit purposes without prior permission or charge. Provided that the authors, title and full bibliographic details are credited, a hyperlink and/or URL is given for the original metadata page and the content is not changed in any way.

---

City Research Online:

<http://openaccess.city.ac.uk/>

[publications@city.ac.uk](mailto:publications@city.ac.uk)

---

# Experimental investigation into the primary fabric of stress transmitting particles

J. Fonseca, C.C. Reyes-Aldasoro  
*City University London, UK*

C. O'Sullivan  
*Imperial College London, UK*

M.R. Coop  
*City University of Hong Kong, HK*

**ABSTRACT:** Understanding the stress distribution amongst the constituent grains is fundamental to predict the response of soil and advance science-based, rather than purely empirical, constitutive models. Photoelastic experiments and discrete element method simulations have provided evidence that, upon loading, discrete force chains form in granular materials. These force chains are made up of particles transmitting relatively large stresses and they are aligned in the direction of the major principal stress. A few qualitative studies have identified the presence of these force chains in sands but direct measurements of force chains have not been previously documented and tracking stress transmission in assemblies of real soil grains remains a challenging task. The present study makes use of three dimensional micro CT images to investigate the evolution of the internal topology of a sand subjected to triaxial compression loading. The analysis of the contact normal and branch vector orientations has shown the realignment of the contact normals in the direction of the major principal stress as a clear indication of the formation of force chains in the post-peak regime. Here the extent of the non-colinearity of the branch and contact normal vectors is explored. Using the micro CT data contact force networks within and outside of shear bands are compared.

## 1 INTRODUCTION

The evolution of internal structure or fabric has a key role in shaping the macroscopic response of granular materials, including soils, to applied loads. If a fabric tensor, describing the contact orientations is known, the overall ensemble properties can be deduced. For example, Thornton (1993) gives a fundamental analytical expression for the overall stiffness of a material that considers the contact stiffnesses and orientations (i.e. fabric). Kumar et al. (2013) demonstrate a constitutive model, whose development was informed by DEM simulations, in addition, the model proposed by Gao et al. (2014) also includes a fabric term. While the veracity of the fabric evolutions predicted or assumed in these models can be tested using DEM, DEM models are limited due to their ideal nature, and so there is a clear need for fabric data to confirm their applicability to real sands.

Granular materials transmit stress through a network of inter-grain contacts, and the fabric tensor describes this network. A key feature of this network is the “strong force chains” which are self-organised column-like structures that form in the direction of the maximum principal stress, each consisting of at least three particles carrying above the global average load (Majmudar & Behringer, 2005; Lin & Tor-

desillas, 2014). Previous studies have suggested that the shear bands that emerge during failure of granular materials are associated with localised buckling of these force chains (e.g. Oda & Kazama 1998). Current understanding of strong force chain behaviour is still largely based on ideal DEM simulations or 2D photoelastic studies.

The current study exploits recent developments in x-ray micro computed tomography (CT) coupled with three dimensional image analysis tools to investigate the network of stress transmission, in specimens of a natural sand. The data presented here will be very useful to understand better the link between fabric and material behaviour in sands.

## 2 MATERIAL AND METHODS

### 2.1 *Reigate sand*

Reigate sand, the material considered here, comes from a formation that is part of the Folkestone Beds (Lower Greensand). In its intact state, Reigate sand is characterised by very high densities and an inter-locked fabric and meets the “locked sand” criteria proposed by Dusseault & Morgenstern (1979). This locked fabric enabled the use of block sampling and so effectively undisturbed samples were considered

in this experimental study, as discussed in more detail in Fonseca (2011).

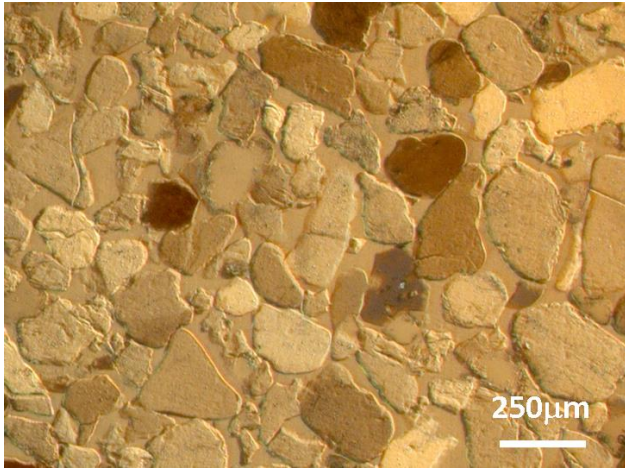


Figure 1. Microscope image of thin section of Reigate sand under polarised light

Reigate is a quartz-rich sand with a median grain diameter of 300 $\mu\text{m}$ . The particle morphology varies from near-spherical grains to highly non-spherical grains with embayments (Fonseca et al., 2012). Note the abundance of long straight and concavo-convex contacts that are evident in the optical microscope image of the intact sand in Figure 1.

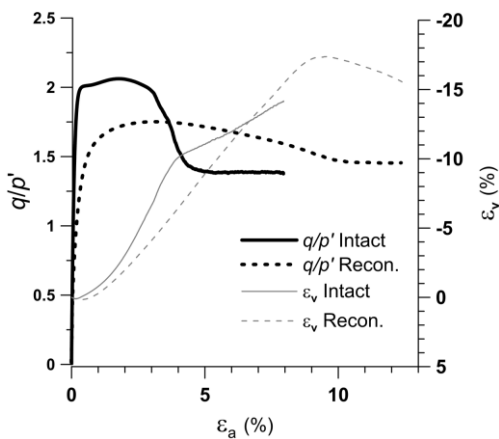


Figure 2. Mechanical and volumetric response for the intact and reconstituted samples.

## 2.2 Test programme and equipment

Triaxial compression tests were carried out on both intact and reconstituted samples of the sand at similar densities in a dry state. The intact triaxial samples were obtained by carefully trimming an initial block of soil. The samples' long axis orientations corresponded to the vertical *in situ* orientation. The reconstituted samples were created using sand taken from the trimmings of the intact samples.

Each sample was isotropically compressed to 300kPa at a rate of 50kPa/hour and then subjected to strain controlled compressive shearing at a rate of 1%/hour with a confining pressure of 300kPa. There are marked differences between the mechanical behaviours of the intact and reconstituted samples,

Figure 2. The intact soil showed a peak strength that is significantly higher than that of the reconstituted soil, and a correspondingly greater degree of strain-softening. The greater peak stress ratio, stiffness and rate of dilation exhibited by the intact material, when compared to the reconstituted soil, have been well documented (e.g. Cresswell & Powrie, 2004). Specimens were observed to fail along a well defined shear plane with an inclination of 63° and 57° (from horizontal), for the intact and reconstituted soil, respectively. In order to investigate the internal microstructure of the soil, the tests were stopped at different stages of loading and the samples were impregnated with resin while in the cell. A low viscosity resin was used to avoid soil disturbance; the impregnation process is discussed in detail by Fonseca (2011). Table 1 summarizes the tests considered here; there are four intact samples (sample reference 'Int') and three reconstituted samples (sample reference 'Rec'). All of the data presented here are for post-peak load stages (Stages 3 and 4) and the relevant strain levels are given in Table 1.

Table 1. Data for the samples investigated ( $\epsilon_a$ =axial strain,  $q/p'$ =deviator stress/mean stress,  $v$ =specific volume)

Sample ref.	Load stage details			Sample location
	$\epsilon_a$	$q/p'$	$v$	
Int-3a	3.89	1.73	1.63	Outside shear band
Int-3bS	3.89	1.73	1.63	Includes shear band
Int-4a	7.94	1.38	1.67	Outside shear band
Int-4bS	7.94	1.38	1.67	Includes shear band
Rec-3aS	9.66	1.46	1.87	Includes shear band
Rec-3b	9.66	1.46	1.87	Outside shear band
Rec-4aS	12.35	1.46	1.70	Includes shear band

## 2.3 3D Imaging process

Small cores (5mm diameter) were extracted from regions containing the shear band and from the bulk of the impregnated triaxial samples. The cores were imaged using x-ray computed tomography (micro-CT) using a *nanotom* (phoenix|x-ray, GE). The voxel size of most of the images was 5 $\mu\text{m}$ , i.e. approximately 0.015 $\times$ d<sub>50</sub>, where d<sub>50</sub> is the median particle diameter. The images were segmented in order to identify the individual grains, each particle-phase voxel was assigned an integer identification number ( $p_i$ ) to associate it to a specific grain (Fonseca et al., 2012). Contacts between two given particles were identified along the boundaries by considering the voxel  $p_i$  number. For two contacting particles, with intensity values  $p_1$  and  $p_2$ , the particle  $p_1$  voxels were classified as contact voxels if they connected to a voxel of value  $p_2$ , where  $p_2 \neq p_1$  and  $p_2 \neq 0$  (as the void space has intensity 0). The voxel contact classification used in this study was based on a 6-connectivity voxel neighbourhood relation, and required a total of six orthogonal 'passes' through the

data along the x, y and z directions (Fonseca, 2011; Fonseca et al., 2013a).

### 3 ANALYSIS OF THE RESULTS

#### 3.1 Orientation vectors

The vectors considered for this analysis were the contact normal orientation (CN) and the branch vector (BV), Figure 3. The vector defining the contact normal was obtained by applying a least square regression to identify a best-fit plane for each surface defining the contact and this plane defined the contact normal orientation. The branch vector is defined as the vector connecting the centroids of two particles in contact.

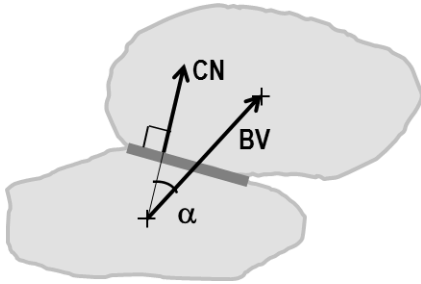


Figure 3. Schematic diagram illustrating the contact normal (CN) and branch vector (BV)

#### 3.2 Angular plots

A convenient away of visualising the distribution of large dataset of vectors is to use rose diagrams. These angular histograms show the orientation of the 3D vectors in a projected plane. In this case the vertical x-z plane was chosen and the angle was measured from the horizontal x-y plane. Each bin is shaded by the average area of the contacts whose normal orientations lie within that bin. For both the contact and branch vectors, the more vertical vectors are associated with the larger contact areas, represented by the lighter bins in the rose plots. Prior to loading the vectors show essentially an isotropic distribution (Fonseca et al., 2013), but as shearing progresses there is a clear reorientation of the preferential contact normal orientation towards the direction of the major principal stress. This trend was observed for both intact and reconstituted samples at load stages 3 and 4 outside the shear band and it is demonstrated here for sample Int-3a in Figure 4(a). The reorientation of these vectors along the direction of the major principal stress supports previous observations from photoelastic tests and DEM analyses on the formation of columns of grains creating chains of transmitted stress. The images in Figures 4 (c) and (g) show clearly that inside the shear band the predominant direction of the contact normals is not always vertical, for example for sample Rec-4aS it is approximately 30° from the vertical

(Figure 4(g)). This observation can be related to the buckling of the force chains which has been pointed as the micromechanism at the origin of the formation of the shear band (Oda et al, 2004; Tordesillas & Muthuswamy, 2009).

In the case of the branch vectors a near isotropic distribution was also observed prior to peak and for stages 3 and 4 (outside the shear band) the reorientation of the BV vectors along the vertical direction is less evident, as shown for stage 4 in Figure 4(b).

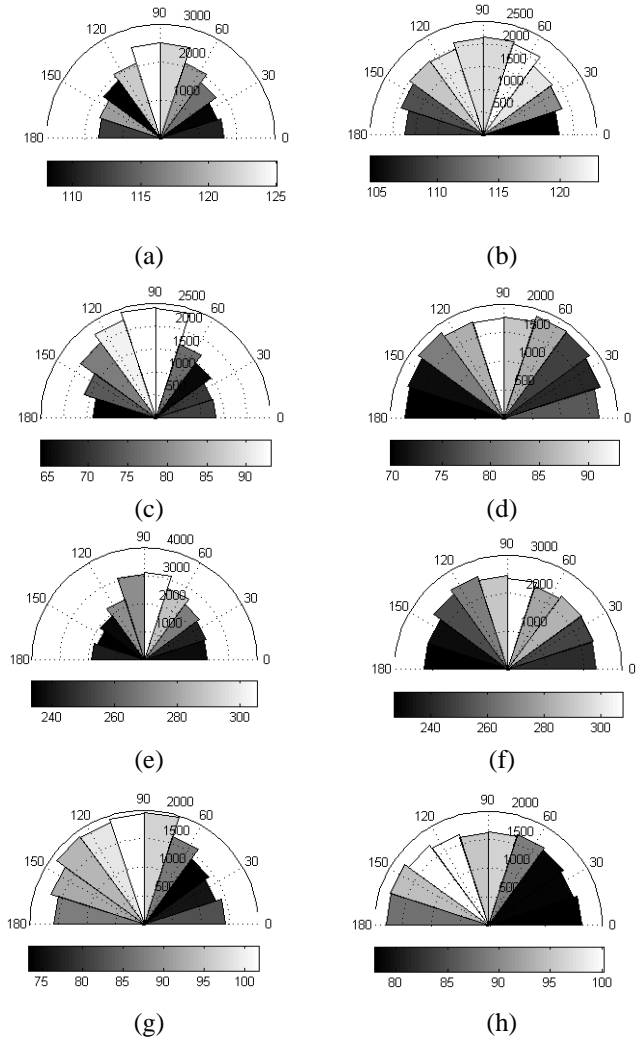


Figure 4. Rose diagrams for specimens at load stage 4 (shading indicates average contact area in  $\mu\text{m}^2$ ); (a) CN Int-3a; (b) BV Int-3a; (c) CN Rec-3aS; (d) BV Rec-3aS; (e) CN Int-4bS; (f) BV Int-4bS; (g) CN Rec-4aS; (h) BV Rec-4aS

The distribution of branch vectors inside the shear band does not translate the buckling phenomenon in terms of generating a clear realignment of the vectors towards the orientation of the shear plane (Figure 4(b), 4(d) and 4(h)). However, the relative movement of the grains inside the shear band can be identified by the rotation of the vectors associated with larger contact area (white bins in the rose plot) as clearly illustrated in Figure 4(h). The main differences observed between the CN and BV data vectors are related to the fact that the BV depends on the on the shape and relative position of the particles in

contact rather than simply in the orientation of the contact itself.

Table 2. Data for the samples investigated

Sample ref.	No. vectors	Fabric tensor parameters			
		$(\Phi_1 - \Phi_3)^{CN}$	$\beta^{CN}$	$(\Phi_1 - \Phi_3)^{BV}$	$\beta^{BV}$
Int-3a	20096	0.088	82	0.061	84
Int-3bS	12906	0.142	72	0.027	64
Int-4a	12200	0.081	89	0.052	87
Int-4bS	24192	0.102	75	0.028	14
Rec-3a	18924	0.143	76	0.022	63
Rec-3b	19674	0.125	86	0.034	23
Rec-4a	17630	0.095	68	0.030	21

Following Satake (1982), a second order fabric tensor  $\Phi_{ij}$  was calculated to investigate the preferred orientation of the dataset of vectors and its associated intensity:

$$\Phi_{ij} = \frac{1}{N} \sum_{k=1}^N n_i^k n_j^k \quad (1)$$

where  $N$  = the total number of vectors in the system and  $n_i^k$  = the unit orientation vector along direction  $i$ .

Fabric tensors were calculated for both the contact normal ( $\Phi_{ij}^{CN}$ ) and the branch vector ( $\Phi_{ij}^{BV}$ ). The anisotropy of the specimen at each load stage was quantified by considering the difference between the maximum and minimum eigenvalues of the fabric tensor, i.e.  $\Phi_1 - \Phi_3$ . The dominant orientation of the dataset was quantified by the angle  $\beta$  given by the major principal eigenvector to the horizontal. The results for the contact normal and branch vector data are presented in Table 2 together with the number of vectors used. The CN data show much higher anisotropy values when compared to the BV which is in accordance with the strong alignment of the vectors observed in the rose diagrams. This trend is slightly more pronounced for the samples outside the shear band. The evolution of the micro-scale parameter  $\beta$  is compared with the macro response given by the stress:strain curves of both the intact and reconstituted soil, Figure 5, for the CN data. The samples outside the shear band, both intact and reconstituted, show  $\beta$  values greater than  $80^\circ$ , i.e. a deviation from the vertical of less than  $10^\circ$ . For the samples including the shear band,  $\beta$  takes slightly lower values, between  $60-80^\circ$ . This is in agreement with what has been shown in the rose diagrams in Figure 4. Similarly to the steady stage reached by the deviatoric stress at stages 3 and 4,  $\beta^{CN}$  also appears to reach relatively stable values for the regions inside and outside the shear band, respectively. For the branch vector data, the distribution of the vectors is more isotropic with no clear predominant orientation, as shown by the rose diagrams, therefore the physical meaning of the fabric tensor parameters  $\beta$  and  $\Phi_1 - \Phi_3$  is less significant.

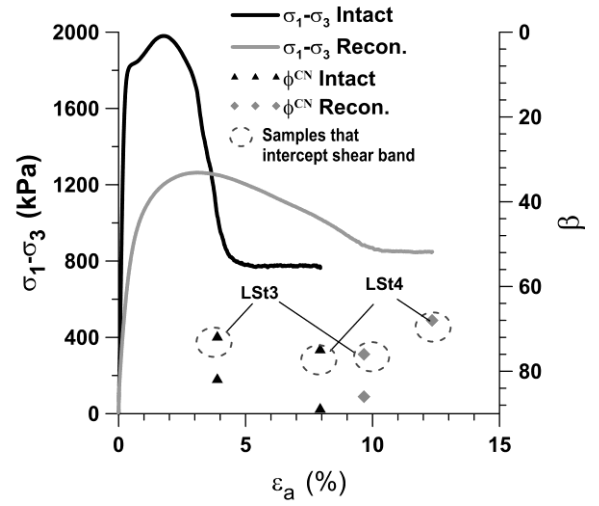


Figure 5. Evolution of major principal fabric orientation for contact normal

### 3.3 Contact normal and branch vector relationship

Typically DEM simulations use ideal circular or spherical particle geometries for which the contact vectors and the branch vectors are collinear. For real soils, however, is not necessarily the case, and in fact they are most likely to be non-collinear as the schematic in Figure 3 shows. In this study, the relationship between the contact normals and the branch vector was investigated by considering the angle  $\alpha$ . Given the high dependency of  $\alpha$  on the morphology of the soil particles, the distribution of  $\alpha$  is presented using rose diagrams shaded by the aspect ratio parameters, elongation index ( $EI$ ) and flatness index ( $FI$ ), the sphericity ( $S$ ) and the contact area ( $CA$ ), this last parameter measured in voxels. The elongation and flatness indices are defined as follows:

$$EI = b/a \quad (2)$$

$$FI = c/b \quad (3)$$

where  $a$  = length of the major principal axis,  $b$  = length of the intermediate principal axis and  $c$  = length of the minor principal axis, obtained using image processing techniques as described in Fonseca et al., (2012).

The sphericity ( $S$ ) was calculated by:

$$S = \frac{\sqrt[3]{36\pi V_p^2}}{SA} \quad (4)$$

where  $V_p$  = particle volume;  $SA$  = surface area of the particle.

As shown in Figure 6 the angle  $\alpha$  varies between  $0$  and  $60^\circ$  with the most frequent value being  $20^\circ$  and this trend is common for all the samples. The effect of grain aspect ratio given by the elongation and flatness indices on the values of  $\alpha$  is shown in Figures 6(a), 6(d) and 6(g). We can observe that as the elongation and flatness indices decrease, and the ge-

ometries deviate from regular spherical shapes,  $\alpha$  increases, i.e. a greater deviation from a spherical shape results in a greater difference between the CN and the BV vectors. The angle  $\alpha$  is also sensitive to the sphericity of the grains in contact (Figures 6(b), 6(e) and 6(h)); for sphericity values closer to 1 (i.e. grain shape close to a sphere),  $\alpha$  takes values closer to 0 as would be expected. Finally a clear trend is also found for the contact area with  $\alpha$  also increasing as the contact area increases, Figures 6(c), 6(f) and 6(i).

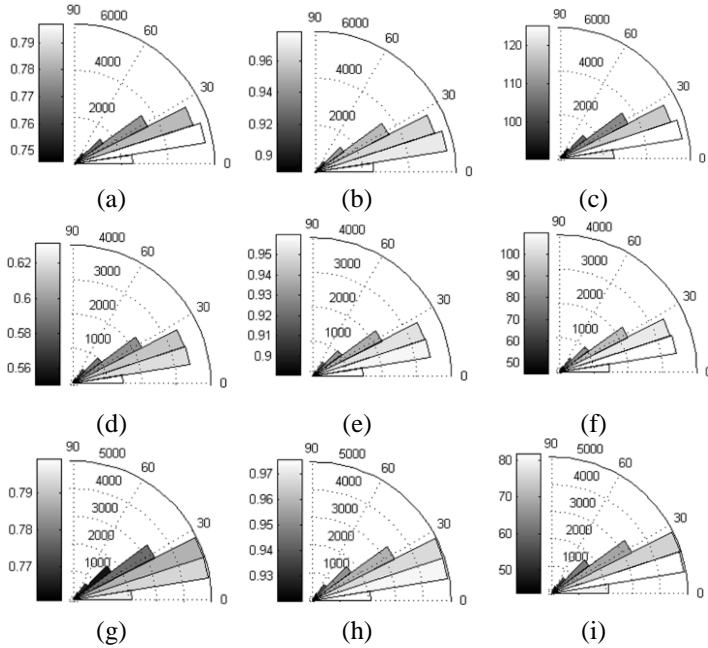


Figure 6. Distribution of  $\alpha$  for the specimens: (a) Int-3a shaded by EI; (b) Int-3a shaded by S (c) Int-3a shaded by CA; (d) Int-3bS shaded by FI; (e) Int-3bS shaded by S (f) Int-3bS shaded by CA; (g) Rec-3a shaded by EI; (h) Rec-3a shaded by S (i) Rec-3a shaded by CA

#### 4 NETWORKS OF STRESS TRANSMITTING PARTICLES

Networks of contacts and contact forces have received considerable interest in recent literature (e.g. Hanley et al., 2014; Lin & Tordesillas, 2014). In these studies, networks represent a collection of nodes and links, nodes are represented by grains and the connecting links are related to the existence of a contact between grains. The contact network can be easily generated by joining the centroids of contacting particles. In the absence of force measurements, this study makes use of geometrical considerations to generate the strong network of stress transmission. It is assumed that these force chains can be identified as being the arrangement of contacting particles whose branch vectors are near parallel to the major principal stress. The intensity of the vectors is given by the contact area, one can infer that larger area contacts are related to more stable force chains that compose the strong force network.

The vectors were obtained by joining the centroids of contacting particles, similarly to what is done in DEM studies. It has been assumed that a condition for a vector to belong to the strong network of inter-grain contacts was to have a near-vertical orientation. Therefore only vectors deviating less than  $45^\circ$  from the vertical (in spherical coordinates) were used. The vectors were allocated into a 3D space of the same dimension as the original image of the sample (i.e. 600 voxels cube) which we call the vectorial volume (VV). Figure 7(a) shows the maximum intensity projections of the VV (calculated for a volume of 50voxels thickness). The magnitude of the vectors was made proportional to the size of the contact area (represented by a lighter colour). These projections were filtered using a low pass filter in order to enhance the selection of the vectors with greater intensity that are, therefore, more likely to belong to the main network of contacts, Figure 7(b). This was followed by the application of a watershed transform to discard shorter and unconnected lines.

The resulting network of the stress transmitting grains is shown in Figure 8(a) for the sample Int-3a, outside the shear band, and in Figure 8(b) for the sample Int-3bS containing part of the shear band. We hypothesise that these quasi-vertical vectors networks are closely correlated to the networks contacting particles that transmit stress. Inside the shear band there is a lower network density, this is in agreement with mechanisms revealed in DEM simulations. The identified force chains are significantly smaller in number and there are fewer connected links meeting our criteria compared with the sample outside the shear band. Considering all the rose diagrams in Fig 4 associated with shear bands, it is clear that while the branch vectors associated with the larger contacts to tend to bend to be orthogonal to the shear plane, there is not a general reorientation of these vectors.

We suggest that the methodology presented here is an effective way to identify different mechanisms of stress transmission for regions of localised deformation. The sensitivity of the technique to different stages of deformation is still under investigation.

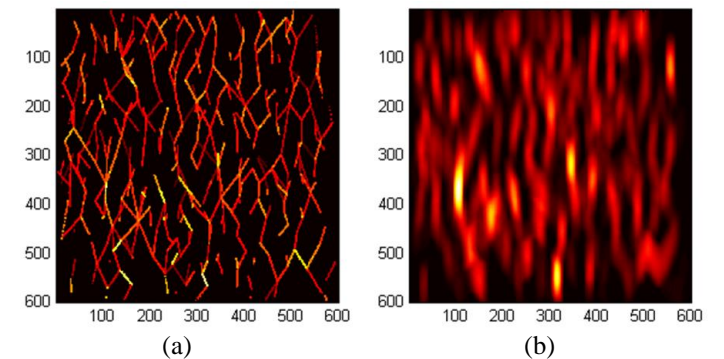


Figure 7. (a) Projection of the 3D vectors, the vectors associated with larger contacts are represented by brighter colours (b) Vectors following the low pass filter.

## 6 ACKNOWLEDGEMENTS

The first author would like to acknowledge the financial support from the Portuguese Government Body, Fundação para a Ciência e a Tecnologia (FCT).

## 7 REFERENCES

- Cresswell, A., Powrie, W., 2004. Triaxial tests on an unbonded locked sand. *Géotechnique* 54 (2), 107–115
- Dusseault, M. B. & Morgensten, N.R. 1979. Locked sands. *Q. J. Engng Geol.* 12, 117-131.
- Fonseca, J., O’Sullivan, C., Coop, M. & Lee, P.D. 2012. Non-invasive characterization of particle morphology of natural sands. *Soils and Foundations* 52(4): 712-722.
- Fonseca, J., O’Sullivan, C., Coop, M. & Lee, P.D. 2013. Quantifying evolution soil fabric during shearing using directional parameters. *Géotechnique* 63(6): 487-499.
- Fonseca, J., O’Sullivan, C., Coop, M. & Lee, P.D. 2013a. Quantifying evolution soil fabric during shearing using scalar parameters. *Géotechnique* 63(10): 818-829.
- Fonseca, J. 2011 The evolution of morphology and fabric of a sand during shearing, PhD Thesis, Imperial College London
- Gao, Z., Zhao, J., Li, X.-S. & Dafalias, Y. F. 2014 A critical state sand plasticity model accounting for fabric evolution. *Int. J. for Num. and Anal. Meths in Geomechanics*, 38 (4): 370-390.
- Hanley, K.J., Huang, X., O’Sullivan, C. & Kwok, F.C. 2014 temporal variation of contact networks in granular materials, *Granular Matter*, 16, 41-54
- Kumanr, N., Luding, & Magnanimo, V. 2014 Macroscopic model with anisotropy based on micro-macro information *Acta Mechanica In Press*
- Lin, Q. & Tordesillas, A. 2014 Towards an optimization theory for deforming dense granular materials, *Journal of Industrial and Management Optimization*, 10, 337-362
- Majmudar, T.S. & Behringer, R.P. 2005 Contact force measurements and stress-induced anisotropy in granular materials, *Nature*, 435, 1079-1082
- Oda, M. & Kazama, H. 1998 Microstructure of shear bands and its relation to the mechanisms of dilatancy and failure of dense granular soils *Géotechnique* 48(4), 465-481.
- Oda, M., T. Takemura, & M. Takahashi 2004 Microstructure in shear band observed by microfocus X-ray computed tomography. *Géotechnique* 54(8), 539-542.
- Satake, M. 1982 Fabric tensor in granular materials. In IU-TAM Conference on Deformation and Failure of Granular Materials.
- Thornton, C. (1993) On the relationship between the modulus of particulate media and the surface energy of the constituent particles *J. Phys. D: Appl. Phys.* 26 1587
- Tordesillas, A & Muthuswamy, M. 2009 On the modelling of confined buckling of force chains *J. Mechanics Physics Solids* 57, 706–727

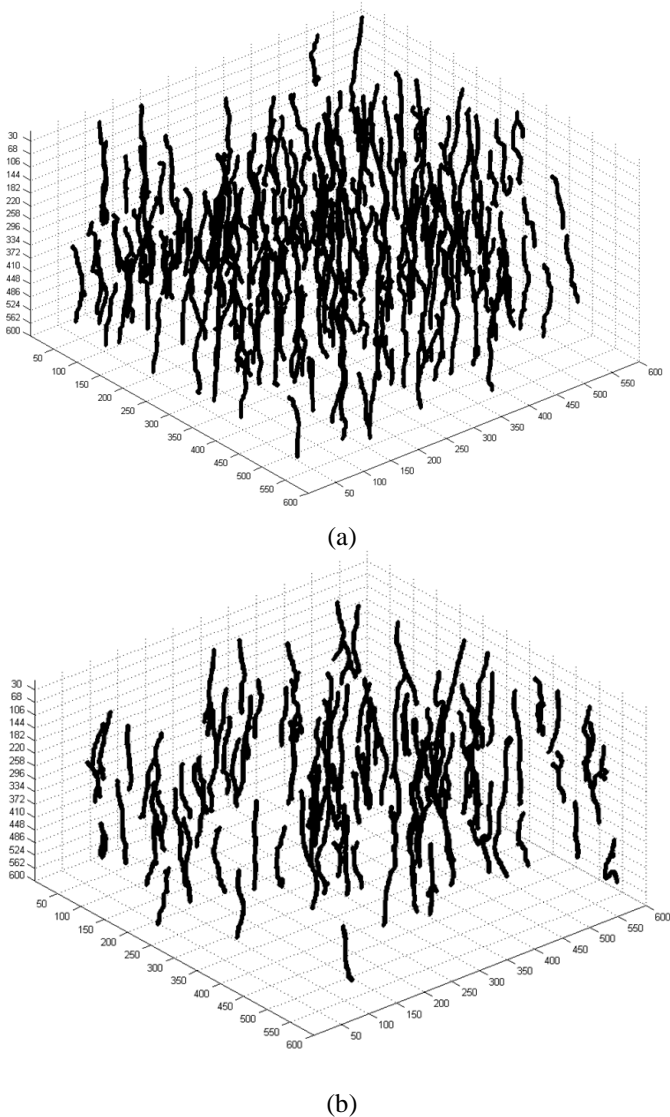


Figure 8. Network of the stress transmitting grains for the samples: (a) Int-3a and (b) Int-3bS

## 5 CONCLUSIONS

This paper presents an investigation into the microscale phenomena occurring in a natural sand on the post-peak regime of shearing deformation. The most striking observation from this study is the realignment of the contact normals in the direction of the major principal stress as a clear indication of the formation of force chains. These quasi-vertical vectors are associated to grains forming large contact areas which compose solid columnar structures of stress transmitting grains. For the regions including the shear band it has been observed the bending or buckling of these columns towards the orientation of the shear plane. This analysis presents unique insights into the influence of contact and grain morphologies on the process of the stress transmission from grain to grain and consequently on the deformation and macro-scale response of the material.